Pellet Injection into ASDEX Upgrade Plasmas

P.T. Lang, H. Zohm, K. Büchl, J.C. Fuchs, O. Gehre,
O. Gruber, R.S. Lang, V. Mertens, J. Neuhauser,
H. Salzmann, ASDEX Upgrade Team, NBI Team

IPP 1/296

April 1996

MAX-PLANCK-INSTITUT FÜR PLASMAPHYSIK

85748 GARCHING BEI MÜNCHEN

MAX-PLANCK-INSTITUT FÜR PLASMAPHYSIK

GARCHING BEI MÜNCHEN

Pellet Injection into ASDEX Upgrade Plasmas

P.T. Lang, H. Zohm, K. Büchl, J.C. Fuchs, O. Gehre,
O. Gruber, R.S. Lang, V. Mertens, J. Neuhauser,
H. Salzmann, ASDEX Upgrade Team, NBI Team

IPP 1/296 April 1996

Die nachstehende Arbeit wurde im Rahmen des Vertrages zwischen dem Max-Planck-Institut für Plasmaphysik und der Europäischen Atomgemeinschaft über die Zusammenarbeit auf dem Gebiete der Plasmaphysik durchgeführt.

PELLET INJECTION INTO ASDEX UPGRADE PLASMAS

P. T. Lang, H. Zohm, K. Büchl, J. C. Fuchs, O. Gehre, O. Gruber, R. S. Lang, V.Mertens, J. Neuhauser, H. Salzmann, ASDEX Upgrade Team, NBI Team

Max-Planck-Institut für Plasmaphysik
EURATOM Association
Boltzmannstr. 2, 85748 Garching, Germany

ABSTRACT

This work comprises results obtained using the new centrifuge injection system for the two first years of pellet injection experiments at Asdex Upgrade until the end of the 1995 experimental campaign. The main aim of the pellet injection investigation is to develop scenarios allowing for a more flexible plasma density control means of injection of cryogenic solid hydrogen pellets. Efforts have been made to develop scenarios allowing more flexible plasma density control by injecting cryogenic solid hydrogen pellets. While the injection of pellets during ohmic discharges was found to be most efficient and also improves the plasma performance, increasing the auxiliary heating power causes a detoriation of the pellet fuelling efficiency. A further strong reduction of the pellet fuelling efficiency by an additional process was observed for the more reactor-relevant conditions of shallow particle deposition during H-mode phases. With injection during type I ELMy H-mode phases, each pellet was found to trigger the release of an ELM and therefore cause particle losses mainly from the edge region. In the type I ELMy H-mode, only sufficient pellet penetration allowed noticeable, persistent particle deposition in the plasma by the pellets. Applying adequate pellet injection conditions and favourable scenarios using combined pellet/gas puff refuelling, significant density ramp-up to densities exceeding the empirical Greenwald limit by up to a factor of two was achieved even for strongly heated H-mode plasmas.

Table of Contents

1. INTRODUCTION

In order to achieve steady-state operation in a future fusion reactor, subsequent delivery of an appropriate amount of fuel into the burning plasma is required. Pellet injection is intended to control the core plasma density in order to maintain the fusion power at the required level, to refuel D (deuterium) and T (tritium), to establish a flow of hydrogenic ions into the scrape-off layer, to reduce the levels of impurities and helium ash, and to promote small high frequency edge localized modes (ELMs) for flushing impurities from H-Mode plasmas. As the T component of the fuel ion mixture of D and T represents a great hazard potential, minimization of the T inventory necessary to achieve steady-state operation in the reactor is required. It has been proposed to reduce the tritium inventory of plasma facing components by isotopic tailoring. In this scenario, T rich pellet fuelling is combined with deuterium rich gas puffing into the divertor or the main plasma. According to computer simulation results, edge tritium fraction can be reduced to 20% to 30% although the DT fuel mixture is about 50% [1,2]. However, for this purpose, a good fuelling efficiency of the pellets is required. If, as indicated by the results presented in this paper, the pellet fuelling leads to the same recycling flux as the gas puff, it cannot be used for a proper isotopic tailoring.

Another encouraging feature of pellet injection is the possibility to overcome the empirical Greenwald density limit. Normally, when refuelling the plasma with gas puffing, the line averaged density cannot exceed the empirical Greenwald limit [3,4]. This limitation would most probably result in a density limit for ITER (EDA) causing problems to reach the required operational density, the regime of detached divertor plasmas, and the H-Mode. One new main intention of pellet injection experiments is therefore to develop scenarios allowing for a more flexible plasma density control and densities beyond the Greenwald limit.

Many experimental studies performed yet on different tokamaks have proven pellet injection to have, under appropriate experimental conditions, the potential of yielding pellet fuelling efficiencies ε_f (plasma particle inventory rise divided by pellet particle content) of almost up to unity [5-8], i.e. almost all the pellet mass is found in the plasma just after injection. In these experiments, it was found that, besides the improved fuelling efficiency, other benefits such as peaked density profiles and enhanced confinement can also be achieved [6,7,9,10]. However, most of these experiments were performed under conditions not likely for a reactor (e.g. pure ohmic heating). Thus, it has still to be investigated whether benefits hitherto achieved with pellet injection can also be realized for conditions similar to those expected for ITER. For

example, a considerable amount of heating power has to be applied and realistic deposition profiles must be chosen. Taking into account the intention to operate ITER in the H-mode regime, pellet refuelling of this plasma mode has to be investigated.
The main aim of our investigations is consequently, to develop possible scenarios for pellet refuelling in the high-confinement plasma regime; the experiments described in this work were performed until the end of the 1995 experimental campaign at ASDEX Upgrade and were mainly dedicated to investigate the features of pellet injection in additionally heated H-mode plasmas. In the experiments performed we injected pellets in a series of discharges with increasing additional heating power; the influence of pellet injection into type I ELMy H-mode discharges is compared with that achieved in ordinary low-confinement plasmas at equivalent heating powers. In this type I ELMy H-mode discharges the ELMs, an MHD instability occurring in the edge of H-mode plasmas, increase their repetition frequency with heating power [11]. It was found that during type I ELMy H-mode phases of a discharge, pellet injection always causes the release of an ELM, with this ELM vice versa affecting the pellet refuelling efficiency.

2. EXPERIMENTAL SETUP

2.1 Centrifuge pellet injector

The pellet injector used on ASDEX Upgrade is a newly developed centrifuge [12] with the capability of varying the pellet velocity (240 to 1200 m/s) and/or mass (1.7 to 4.3 x 10^{20} particles) in order to allow a variation of the deposition profile. Cubic pellets formed from pure hydrogen or deuterium were injected horizontally from the torus low-field side at the midplane of the standard single-null plasma configuration, tilted 11^{o} from the radial direction. Injection was performed at repetition rates of up to 80 Hz, either as pre-programmed sequences or feedback-controlled via the ASDEX Upgrade plasma discharge control system [13] to achieve density control by the pellets.

2.2 Diagnostics

Pellet ablation and penetration are monitored by several CCD cameras (time resolution 10 ms) and photodiodes (max. temporal resolution 2μs) measuring the H_α/D_α (Balmer alpha, n=3 → n=2 transition; centred at 656.5/656.1nm) light emission. A pellet light barrier detector array, mounted at the centrifuge exit to determine the exact flight path of the pellet, together with the pellet CCD picture, allows one to determine whether the pellet enters the discharge as a whole or split into several pieces. Due to the present lack of a pellet mass detector, the proper conservation of the pellet mass was checked by comparing the measured penetration depths Δ of each pellet with a scaling law found for penetration depths in ASDEX [14], adapted for ASDEX Upgrade [15]. This way, pellets showing too little penetration with respect to the scaling law were not considered for further analysis. Pellets yielding penetration depths in the vicinity of the scaling law were taken into account with their design mass; thus, all fuelling efficiencies presented in our analysis underestimate the values actually achieved. From the testbed campaign it is known that the pellet injection velocity can be calculated very precisely (less than 0.3% error!) from the centrifuge revolution period; analysis of the 94 chord signals of the soft X-ray cameras located nearby showed that the pellet injection path never exhibited any significant change of the pellets radial velocity along its flight path in the plasma as well.

2.3 Operating conditions

For all pellet injection experiments, ASDEX Upgrade was operated in a lower single-null divertor configuration (R_0=1.65m, a=0.5m, κ=1.7, V_{Plasma}=13m^3) . For plasma heating, besides ohmic heating, a four-beam NI injector able to produce a ´staircase´ power waveform, was applied.

Use was made of the different H-mode power thresholds for the two directions of the ion ∇B drift [16] to change the confinement regime for a dedicated heating power P_{heat} at a given magnetic configuration by changing the sign of B_T.

Numerous diagnostics were used to study the plasma behaviour [17]. For example, line-averaged electron densities were measured by an eight-chord DCN laser interferometer; the plasma particle inventory and Abel-inverted density profiles were calculated by means of these data. For checking and, in cases where fringes were missed, correcting the interferometer data, three bremsstrahlung detection systems are available. A microwave reflectometry system was applied for density measurements at the plasma edge. Langmuir probes flush-mounted in the divertor target plates and a thermographic system provided information on particle and heat flux into the divertor. Several manometers, placed throughout the vessel, measured the neutral gas pressure. Electron temperatures were determined by Thomson scattering and electron cyclotron emission (ECE). Furthermore, data provided by the electromagnetic probes and several spectroscopic diagnostics were extensively used during this analysis.

3. RESULTS

The experiments reported were performed with the intention of studying the behaviour of pellet-refuelled discharges with increasing heating power and especially when the H-mode regime is entered. In the course of our investigation, the fuelling efficiency ε_f, experimentally determined from the pellet-induced particle inventory increase about 1 ms (temporal resolution of the DCN interferometer) after pellet ablation, turned out to be a key parameter indicating the pellets' effect on the discharge.

3.1. Injection into ohmic plasmas

Fuelling efficiencies close to unity and accordingly a strong influence on the discharge behaviour were found for pellet injection into ohmic plasmas ($P_{OH} \approx 1$MW). Those experiments, performed mainly for testing and demonstrating the capability of the newly developed centrifuge injector, showed almost the same basic results as obtained in similar experiments in other tokamaks, e.g. DIII-D [18], TFTR and JET [19] or ASDEX [7]. Comparing the dynamic ablation profile obtained from the H_α/D_α signal [20,21] with the increment of the radial density profile a few ms after the ablation process showed nearly all pellet material to be confined just where it had been deposited. Successful density buildup to the density limit was possible by repetitive injection of pellets at an adequate rate. When comparing equivivalent discharges at same edge densities, pellet fuelled density limit discharges showed the same scenario causing the disruption than gas puff density limit discharges. In both cases, first a marfe developes in the vicinity of the X-point at high electron densities nearby the separatrix. Close to the density limit, the marfe becomes locally unstable and starts to moves quickly upwards to the high field side, accompanied by mode locking followed up by the major disruption [22]. The electron density profiles temporal evolution for two density limit discharges of identical magnetic configuration (I_P=0.8MA, B_t=-1.35T, q_{95}=2.7)) are shown in Fig. 1a, the left one (#2627) for gas puffing only, the rigth one for refuelling only by pellet injection (#2725, repetition rate 1/75ms; $\Gamma = 3 * 10^{21}$ at/s). Obviously, pellet refuelling causes strong peaking of the density profile. Whereas the value $n_e(0)/n_e(0.95a)$ remains nearly constant during the density ramp up of the gas puff case, i.e. the density profile growth self-similar, $n_e(0)/n_e(0.95a)$ is increased by a factor of 2.5 in the pellet case. Thus, as the edge density governing the density limit, pellet refuelling allows for higher particle inventories than gas puffing and hence gives access to operational parameters beyond the gas puff density limit. For example, a value of $\overline{n_e} = 13 * 10^{19} m^{-3}$ for the line averaged density, which

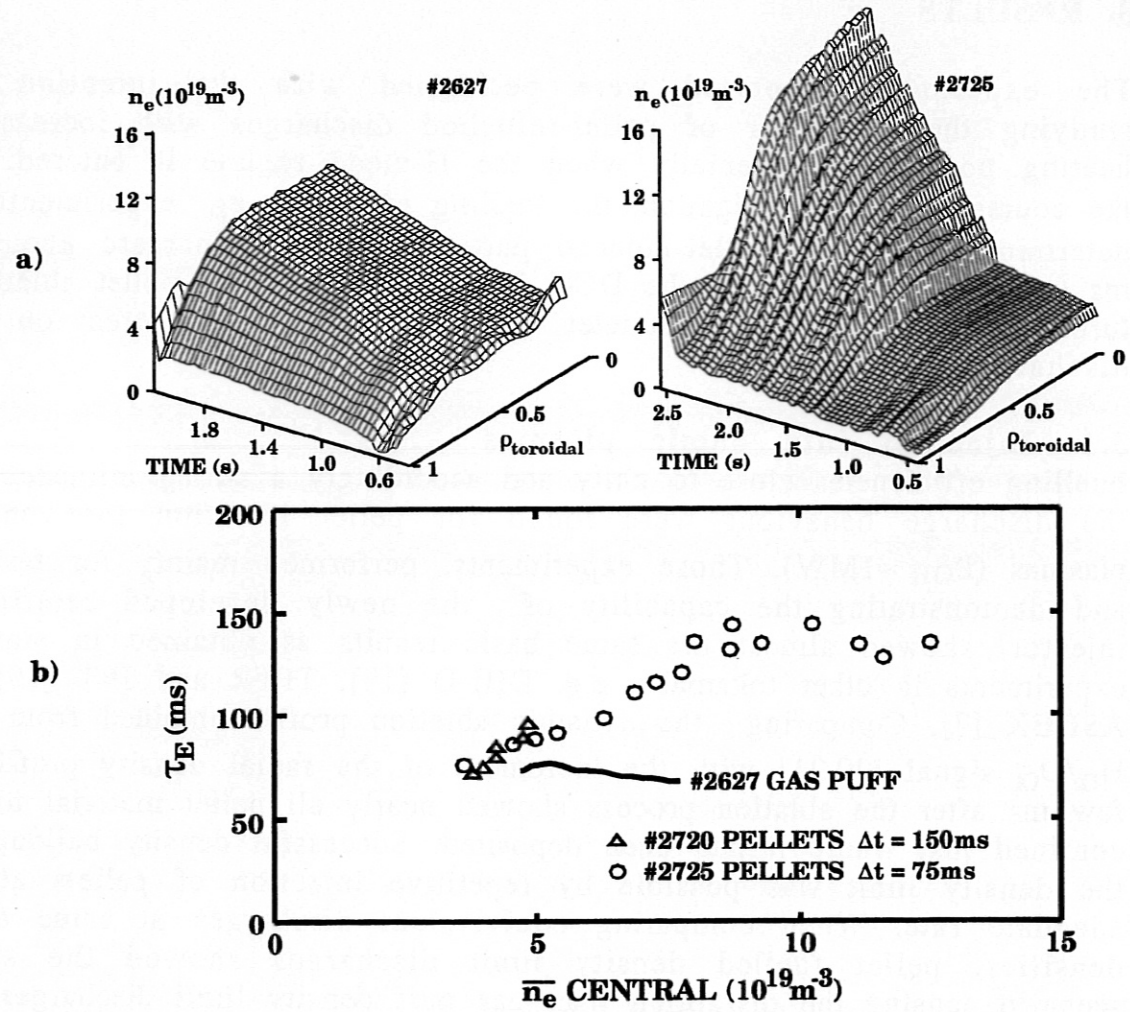

Fig.1: a) Density profile evolution for density limit discharges refuelled by strong gas puffing (left) and pure pellet refuelling at 75ms repetition time; both OH discharges with I_P=0.8MA, B_t=-1.35T and q_{95}=2.7.
b) Energy confinement time calculated from MHD data versus line averaged density for both shots shown in a) and also for pure pellet refuelling at 150ms repetition time.

corresponds to a Murakami parameter of $15*10^{19}m^{-2}T^{-1}$, is reached for #2725. The corresponding data from the equivalent gas puff discharge #2627 were $\overline{n_e} = 7.5*10^{19}m^{-3}$ and $8.8*10^{19}m^{-2}T^{-1}$.
For the central density rises although the pellet penetration depths Δ is less than half of the plasmas minor radius (Δ from 20 to 25cm), the observed peaking of $n_e(r)$ cannot be attributed to central deposition of particles. Hence, our experiments clearly show a change of the particle transport as already found for ASDEX [7]. n_e peaking is caused by an

increasing ratio of the inward pinch velocity v_{in} to particle diffusion coefficient D. Neglecting source terms, this ratio can be calculated using

$$\frac{v_{in}}{D} = \frac{\nabla n_e}{n_e} + \frac{\Gamma_e}{D\, n_e}$$

with Γ_e the radial particle flux density. Investigations using the 1D-radial ASTRA transport code [23] showed the term $\Gamma_e/D\, n_e$ to become very small inside about 2/3 of the plasma radius for times some ms after pellet ablation. Therefore, $\nabla n_e/n_e$ approximates the ratio v_{in}/D fairly well, showing a strong increase during the pellet sequence while in the gas puff case this ratio sticks almost to zero. For a pellet repetition rate reduced by a factor of 2 (#2720, rep. rate 1/150ms), this strong increase of v_{in}/D is no longer observed and only a moderate transient increase of density occurs during the injection sequence. No strong persistent peaking takes place and the discharge does not encounter the density limit.
Adequate pellet refuelling can, beside density peaking and an extended operational regime, also yield better confinement both for the energy and the particles. The energy confinement time, as yielded by an analysis performed for the gas puff and the pellet injections at different repetition rates, is plotted versus the line averaged density in Fig. 1b. For this analysis, the energy confinement time τ_E,

$$\tau_E \equiv \frac{W_{MHD}}{P_{OH} - \frac{\partial W_{MHD}}{\partial t}}$$

(W_{MHD} is the energy content from the magnetic data; P_{OH} is the ohmic heating power; there is no correction for radiation) was calculated in the pellet case only just before a pellet injection. At this time, the reheating of the plasma after pellet injection to the initial value (and also the same profile) was almost finished, loop voltage and ohmic heating power has stabilized near the pre-pellet value and the plasma energy content is nearly constant again. As can be seen from Fig. 1b, with respect to the gas puff case, the higher pellet repetition case doubles the energy confinement time whereas for the less repetition only a marginal increase can be achieved. This behaviour can be interpreted as restoring the situation in the linear part of the $\tau_E / \overline{n_e}$ curve by the pellets up to $\overline{n_e}$ values where the normal gas puff data show already saturation of τ_E. A

detailled discussion of this question has already been given in [7], where discharges showing criteria like these were identified as HRP (high recycling pellet) plasmas showing high recycling at the plasma boundary. This is also consistent with our observation of a significantly reduced neutral gas pressure for pellet refuelling.
A particle transport analysis in ASDEX Upgrade was performed by modelling the time evolution of the DCN chords [24], using the method of solving the particle conservation equation for the equilibrium and linearization for small perturbations to the equilibrium [25]. This analysis yields an increase by a factor ten for the v_{in}/D ratio and from a particle confinement time τ_P of 20ms to 33ms during the pellet sequence of #2725. Being rather uncertain for the absolute values, the analysis however confirms a strong enhancement also in τ_P by pellet refuelling.
It should be mentioned further that for #2725 a strong toroidal deflection, increasing during the pellet sequence, was observed.
As for the pellet repetition rate applied during the discharge #2725 only resulted in a moderate decrease of the T_e profile and pellet penetration depths stayed almost constant, for even higher pellet repetition rates the situation may become different [15]. For a shot (#4238, I_P=0.8MA, B_t=+1.7T, q_{95}=3.4) where 560 m/s pellets were injected at a repetition rate of 1/35ms, strong persistent cooling of the plasma is initiated followed up by a successive deeper pellet penetration. Thus, pellets finally reach the q=1 surface, triggering strong localized density perturbations, referred to as a ´snake´ [26].

3.2. Injection into NI heated plasmas

With the intention to search for conditions where similar beneficial behaviour as found under adequate conditions in OH discharges, the experiments were extended to plasmas with additional heating power applied by neutral beam injection. It turned out, however, the favourable behaviour observed for ohmic heating only (P_{NI}=0) is lost. This is illustrated in Fig.2, where experimental values of ε_f are plotted versus the applied additional heating power, triangles indicating pellets injected during L-mode phases (or in OH discharges), circles injection in H-mode plasmas. Appropriate experiments were performed by injecting sequences of a few pellets at a low repetition rate, not changing the target plasma too strongly by the pellets themselves, into discharges heated with varying neutral beam heating power. The solid line in Fig.2, representing the fuelling efficiency achieved under optimum conditions (most likely nearly "perfect" pellets), shows the strong fuelling efficiency degradation with increasing heating power. Thus, in our

experiment, a maximum fuelling efficiency of only 0.3 could be achieved with about 7MW of NI heating power. The degradation of ε_f with increasing additional heating power has already been reported for many other tokamaks [27-32]. According to investigations performed on JET and TFTR [19], but also to analysis of data from ASDEX, the ε_f degradation is accompanied by a growing shift of the effective deposition profile towards the separatrix. With increasing P_{heat}, a growing discrepancy between the dynamical ablation rate profile, reconstructed by mapping the H_α/D_α emission from the ablating pellet onto the radial location of the pellet trajectory, and the effective ablation rate profile, determined from the change in the density profile, was observed.

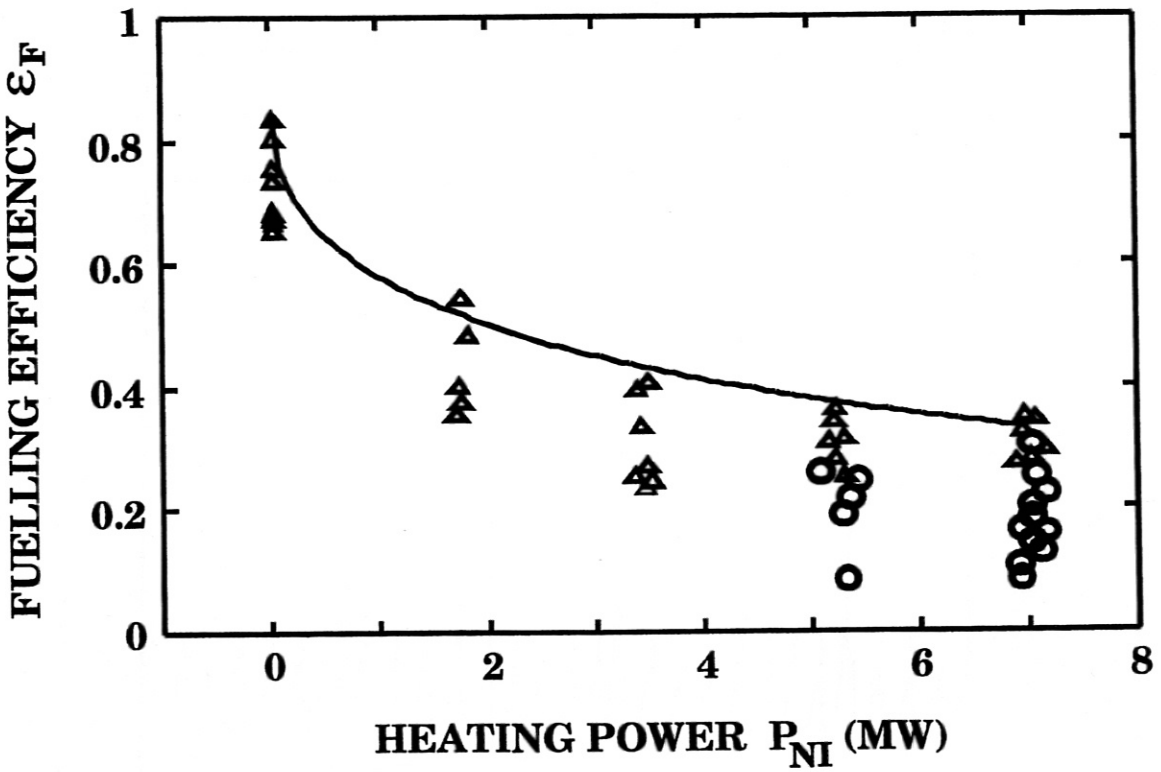

Fig. 2: Pellet fuelling efficiency versus applied additional heating power, ε_f is calculated assuming nominal pellet masses. Triangles: pellet injection during L-mode phases or into ohmic plasmas; circles: H-mode target plasmas; solid line: limiting curve of maximum fuelling efficiency, representing ε_f (P_{NI}) obtained for ideal conditions (e.g. nominal pellet mass).

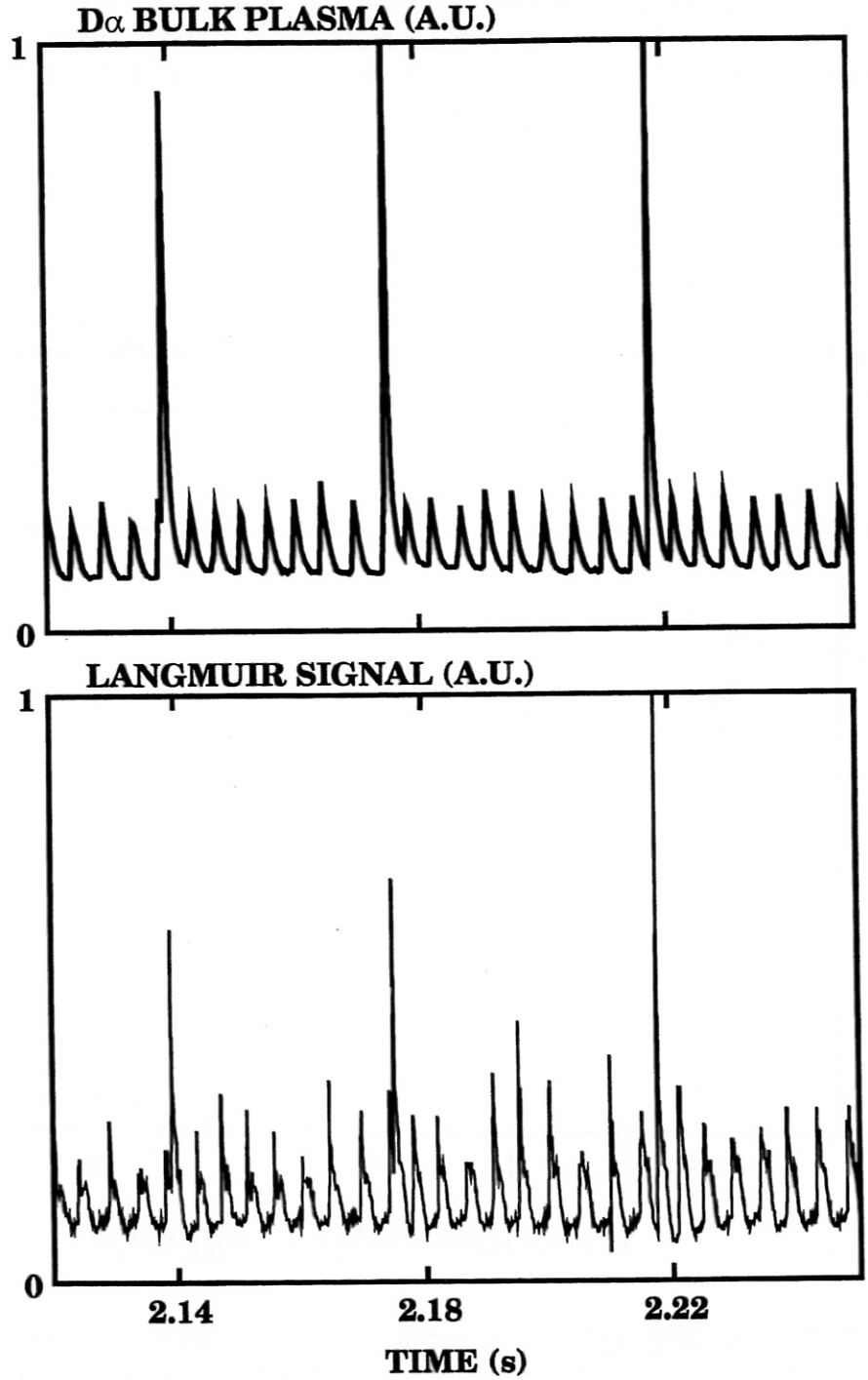

Fig. 3: $D\alpha$ and Langmuir probe signals showing a strong density increase near the divertor plate following pellet injection; this indicates the strong pellet-induced particle flux from the plasma.

For pellets injected into strongly heated plasmas (P_{NI} > 5MW), there is an immediate (temporal resolution about 1ms) onset of strong particle flux following pellet injection, as detected by the reflectometer and - as shown in Fig.3 - by the Langmuir probes mounted in the divertor plates. From the neutral gas gauge signals also the amount of particles expelled by this pellet-induced flux was confirmed to be close to the pellets´ initial mass.
Video observations of the area near the pellet injection port, like in Fig.4, show the expelled material not to be isotropically distributed but still concentrated in a small tube at the plasma edge (∅ few cm) toroidally following the magnetic field lines. Mapping the observed luminiscent structures onto the magnetic field structure confirmed also sticking of the plasmoid to the field lines. Fig.4a and 4b, taken during pellet injection into discharges with reversed toroidal field direction (∇B drift upwards in Fig.4a, downwards in Fig.4b) clearly visualizes the according change of field line helicity. A test observation performed for a colder ohmic plasma (Fig.4c) only showed the ablation trace along the pellet path; no structures corresponding to those observed in pellet injection into strongly heated plasmas were found.

3.3 Injection during type I ELMy H-mode phases

For our efforts made on achieving efficient refuelling for density rampup or even controlling for additionally heated plasmas in the high confinement regime, more problems than the power degradation were enfaced. When injecting slow and small pellets during type I ELMy phases, a further reduction beyond the ε_f degradation with P_{NI} takes place. The reduced fuelling efficiency during the H-mode phase of a discharge could be clearly observed for a shot undergoing several transitions from H- to L-mode and vice versa while the pellet sequence was injected. The discharge (#4292, I_P=0.8MA, B_t=2.0T, ∇B drift downwards, q_{95}=4.0, P_{NI}=7.5MW) was performed for investigations on radiative edge cooling, undergoing several H-L transitions due to strong radiative losses caused by the neon puffed into the plasma at 2.5s. Figure 5 shows that part of the discharge´s temporal evolution where the first backtransition to the L-mode takes place. While the radiation power increases, ELMs indicated by the D_α signals disappear and the plasma energy content reduces. Pellets, clearly indicated by the bulk D_α signal (photodiode viewing pellet entrance sector), obviously cause stronger enhancement of the line-averaged densities (more pronounced in the edge than in the central chord) for the L-mode than for the H-mode. Analysis of the plasma particle inventory showed that particle inventory enhancements by the pellets corresponding to an ε_f of nearly

Pellet ablation
Expelled material
a
b
c

Fig. 4(left): a,b) Video frames taken during pellet injection into NI heated plasmas (B_t=2.5T; P_{NI} = 7.3MW in a); P_{NI} = 3.7MW in b)), showing expelled material (indicated by luminescent region) concentrated within a tube of few cm in diameter following magnetic field lines. Changing the toroidal field direction (∇B drift upwards in a); ∇B drift downwards in b)) accordingly alters the helicity of field lines. c) No similar structures are present in a colder pure ohmic discharge. In this case the video frame shows only the ablation along the pellet path.

0.3 are achieved during the L-mode phase, whereas only about half of this value is obtained during the type I ELMy H-mode without Ne puffing before 2.5s. This behaviour cannot be attributed to different deposition profiles since the measured dynamic ablation profiles and penetration depths (approx. 15cm) were almost identical for all pellets, irrespective of whether they were injected during L- or H-mode phases. This is due to the fact that neither edge profiles of the electron temperature nor the density are changed significantly by the mode transitions during radiative boundary discharge phases [33].
Pellets injected in this discharge - and also into other discharges with strong additional heating - showed no significant influence on the energy confinement time, either during L- or H-mode phases.
The H-mode degradation of the fuelling efficiency was found to show strong dependence on the penetration depths of the injected pellets. When slow (240m/s) and small pellets were injected into H-mode discharges, yielding only very shallow deposition (penetration depths $\Delta \approx$ 8cm) of the fuel, no detectable increase of the line-averaged density and hence the particle inventory could be found. From the fluctuation level of the $\overline{n_e}$ signals an upper limit of 0.08 could be estimated for ε_f. Increasing the penetration depths by increasing the pellet velocity and/or mass yielded an enhancement of the fuelling efficiency. For the H-mode phase of shot #4292, described before, $\varepsilon_f \approx$ 0.15 was achieved for $\Delta \approx$ 15cm. Using the full available potential of our centrifuge both in pellet mass and velocity, at $\Delta \approx$ 25cm almost the L-mode fuelling efficiency is re-established in H-mode plasmas. Fuelling efficiencies, as measured for pellet injection into NI-heated plasmas with P_{NI} = 5-7.5MW and I_P = 0.8-1.05MA, are plotted versus the penetration depths in Fig.6. As can be seen from this plot, H-mode fuelling efficiencies rise with increasing pellet penetration depths until they reach L-mode values at $\Delta \approx$ 25cm; contrary to this behaviour, the fuelling efficiency in L-mode discharges is rather less affected by differing deposition profiles.

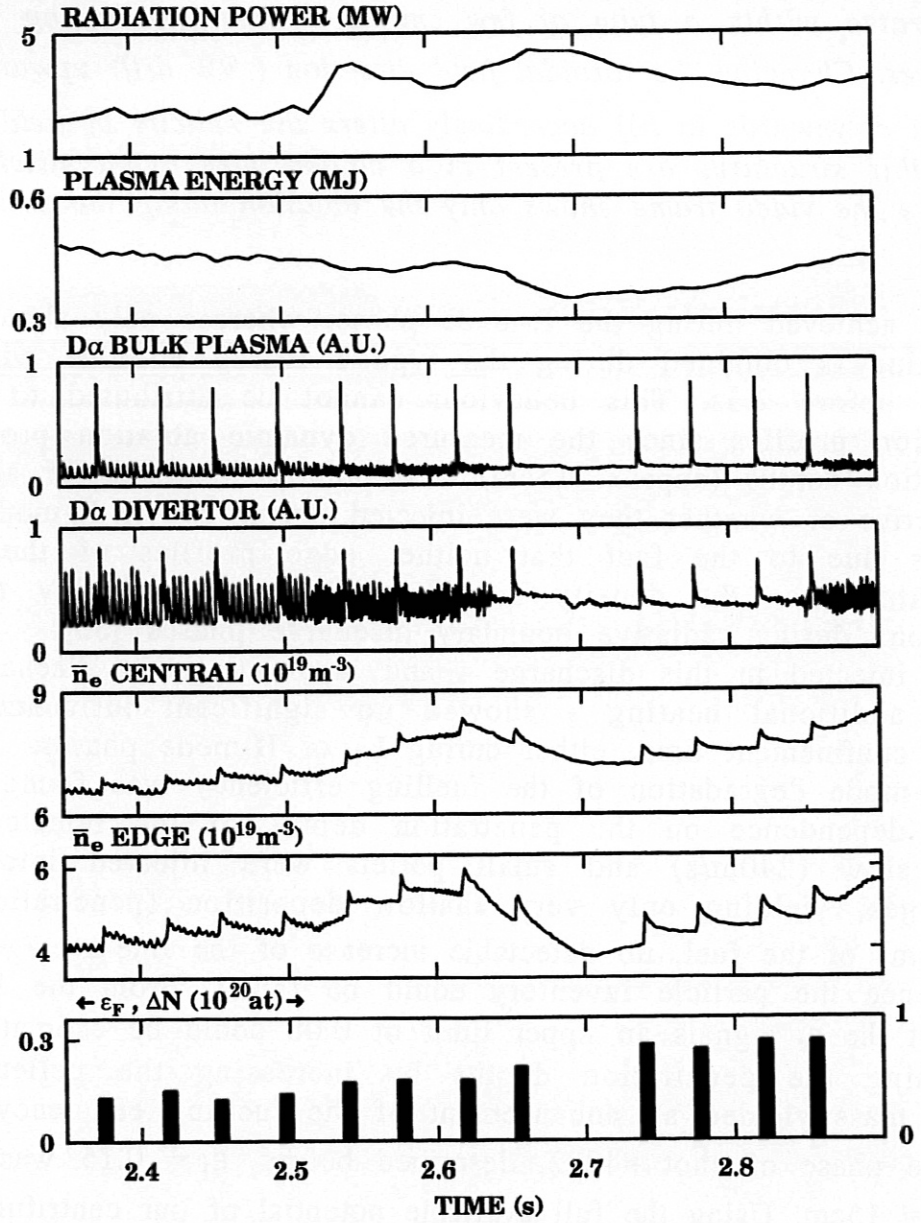

Fig. 5: Time evolution of radiated power, plasma energy content, $D\alpha$ from bulk plasma near the pellet entrance and from the divertor, central and edge line-averaged densities and particle content improvement by each pellet for a discharge (#4292, I_P=0.8MA, B_t=2.0T, q_{95}=4.0, P_{NI}=7.5MW, ∇B drift downwards) sequence with pellet injection during H- to L-mode transition caused by Ne puff at 2.5s.

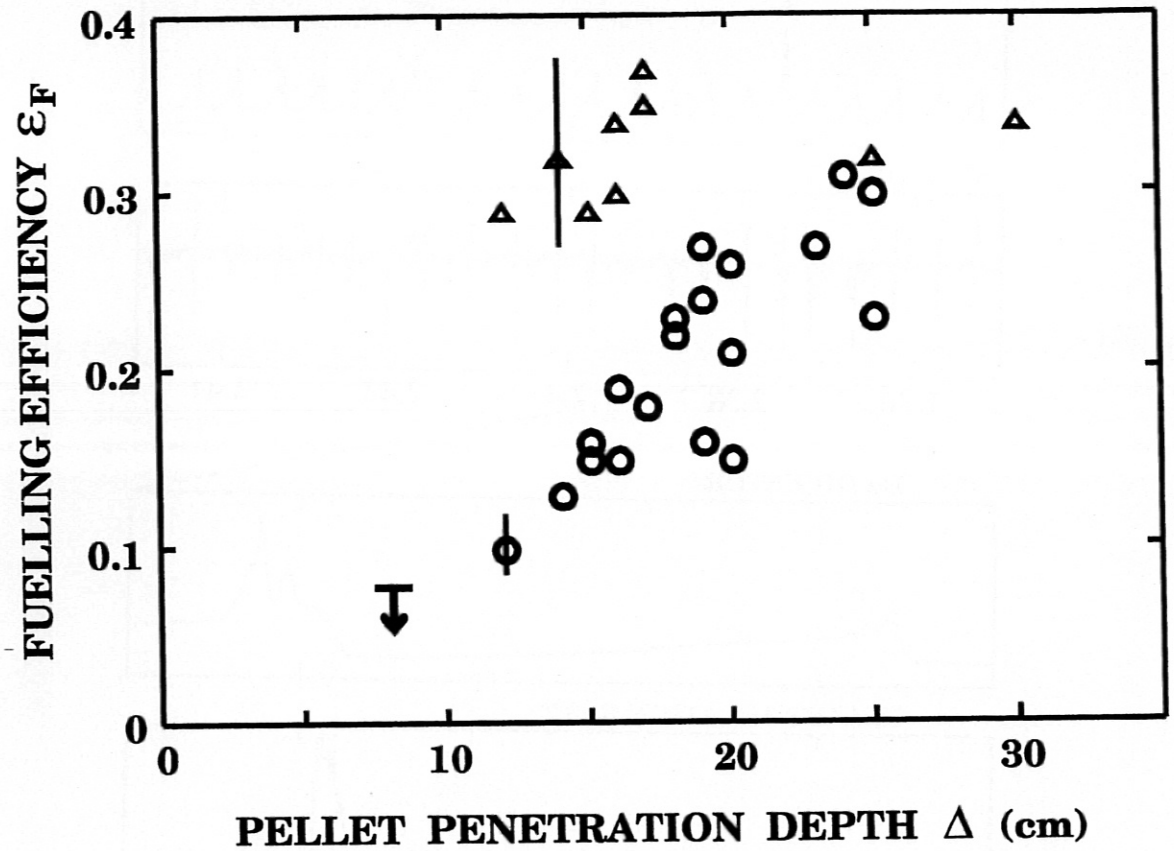

*Fig. 6: Fuelling efficiency (calculated assuming m_P=0.85*nominal pellet mass, estimated error from pellet mass uncertainty indicated by error bars) achieved for a discharge with P_{NI}=5-7.5MW and I_P=0.8-1.05MA, plotted versus the pellets penetration depths into the plasma. Circles: pellets injected during H-mode phases; triangles: L-mode conditions.*

In the search for mechanisms responsible for the strong ε_f degradation in the case of shallow pellet fuelling of H-mode plasmas, an instructive observation was made. Each pellet - no matter whether small or big, or how high or low the velocity - injected during an H-mode phase was found to trigger an event showing a signature almost identical to that of an ELM. As an example, the D_α radiation signal from the divertor, showing the regularly occurring ELMs and also the arrival of pellets, and the MHD mode activity, indicated by the Mirnov coil signal, are shown in Fig.6. During H-mode phases of the discharge, each pellet causes a burst on the MHD trace similar to those resulting from an ELM. On an expanded time scale, shown in the lower part of Fig.7, where the

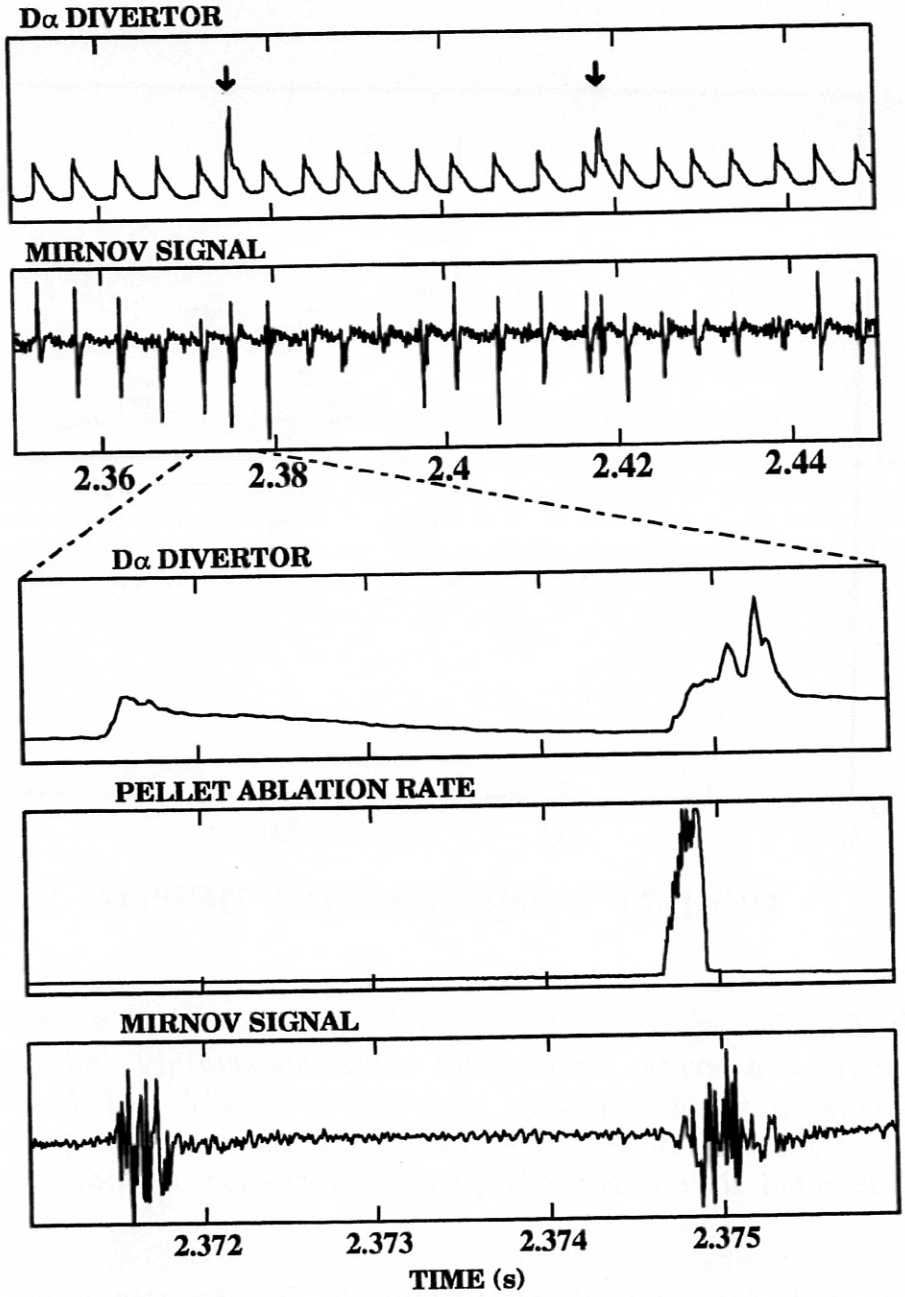

Fig. 7: Dα radiation from the divertor and MHD activity detected by Mirnov coils located below the strike point (#4292, see also Fig.6), indicating triggering of an ELM event by injection of a pellet. The pellets are indicated by arrows.
At an enhanced temporal resolution (lower part) a temporal delay of the pellet-induced ELM signature with respect to the onset of ablation can be recognized. The pellet penetration depth is approximately 14cm for this pellet.

temporal evolution of the pellet ablation rate is also given, it becomes clear that the ELM triggered by the pellet shows some time delay ($\Delta t \approx 100\mu s$) with respect to the start of ablation. For the case shown here (medium pellet mass and velocity, $\Delta \approx 14cm$), the pellet-induced ELM seems to be somewhat longer since the intensity is the same as for a regular ELM. For shallow refuelling (small and slow pellets) with no detectable density enhancement, pellet-induced ELMs were found to have almost no time delay with respect to the ablation onset. Full power injection (maximum pellet size and speed, almost same pellet fuelling efficiency as in L-mode) causes Mirnov activity much stronger and longer than an ordinary ELM. In this case, no noticeable time delay in the ablation onset is found, it perhaps being disguised by MHD activity resulting from a strong plasma motion caused by the pellets.
ELMs remove both energy and particles from the plasma. These losses, affecting mainly the plasma edge region, occur during a period of a few milliseconds. Since the H-mode ε_f degradation was observed to be strongest for pellet particle deposition in the ELM-affected region, it seems reasonable to conclude that strong particle losses taking place under these conditions are caused by the ELM. To understand why each pellet triggers an ELM when injected while the plasma is in the H-mode state and why particle losses during such a pellet-induced ELM can be much bigger than those caused by an "ordinary" ELM, a modelling of this process was performed as described in the section 4.2.

3.4. Pellet refuelling of type I ELMy H-mode discharges

Injecting pellets with penetration depths sufficient for high fuelling efficiency, density ramp-up is possible even for NI-heated plasma discharges during H-mode phases. Using pure pellet refuelling, feedback control of the line-averaged plasma density was demonstrated. In Fig. 8, part of the temporal evolution of a discharge (#5477, I_P=1.0MA, B_t=2.5T, ∇B drift upwards, q_{95}=3.9, P_{NI}=7.5MW) is presented where the line-averaged plasma density was intended to be adjusted during the period from t=2.05 to 2.65s to a value of 8×10^{19} m^{-3}. Pellet injection was controlled during the whole sequence by the plasma discharge control computer. The pellet request signal from the computer is shown by the lower trace prompting the injection of pellets whose arrival at the plasma is indicated by strong spikes on the D_α emission (middle signal trace in Fig. 7). Gas puffing, used earlier in the discharge for density build-up, was completely stopped at t=1.5s; the line-averaged density then remained almost constant at 6×10^{19} m^{-3} till the beginning of pellet injection. With the pellets, the envisaged density ramp-up to 8×10^{19} m^{-3} could be reached within 200ms at a mean pellet repetition rate of 45Hz, equivalent to a mean particle flux of 2×10^{22} at/s. During the

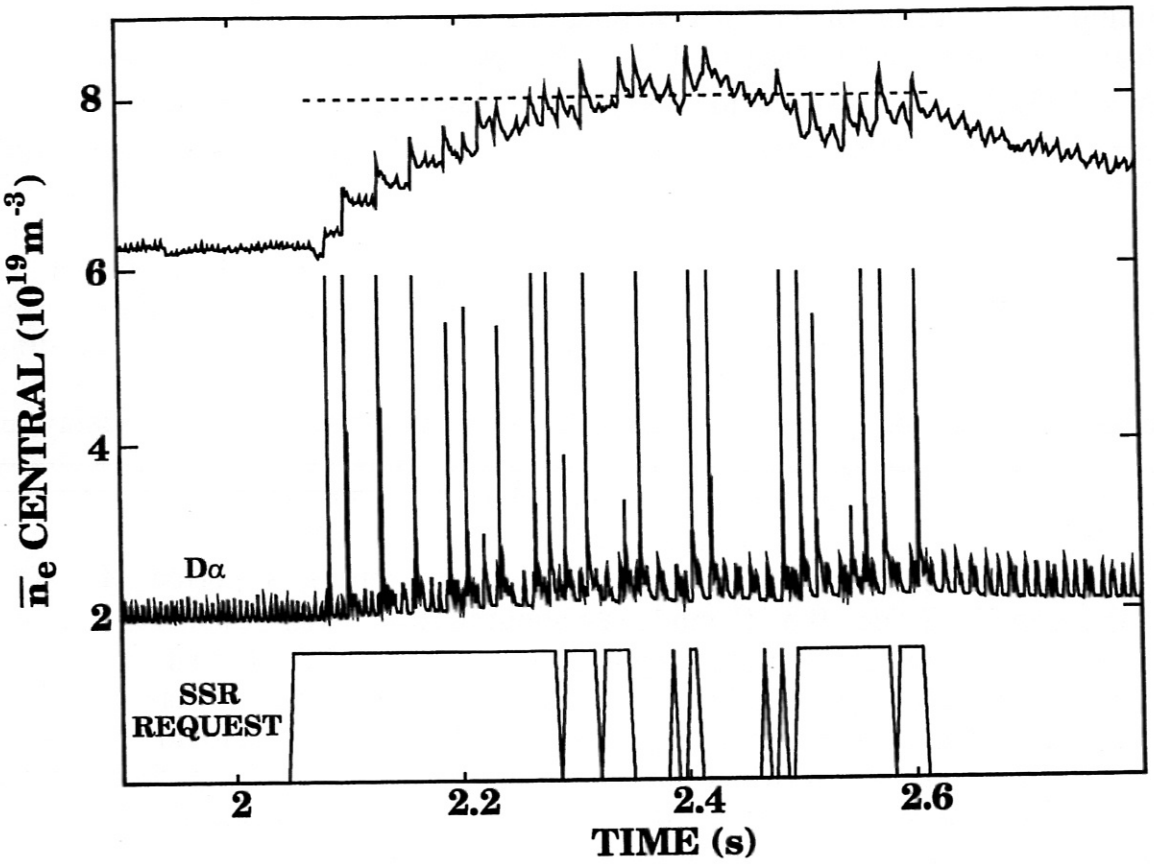

Fig. 8 Density ramp-up and control by pure pellet refuelling. The line-averaged density (upper trace) is adjusted for the period from t=2.05s to t=2.65s to an envisaged value of $8x10^{19}$ m^{-3} by pellet injection (indicated by spikes in the Dα signal, middle trace), controlled by the ASDEX Upgrade plasma discharge controlling computer.

rest of the period, $\overline{n_e}$ was kept almost constant at the required level; after the end of the pellet refuelling, $\overline{n_e}$ begins to decay towards the pre-pellet value.

With the above knowledge of the effect on the fuelling efficiency by pellet-induced ELMs, an attempt was made to optimize density enhancement for H-mode discharges refuelled by pellets of maximum size and velocity. It turned out that simply replacing the gas puffing by pellet injection does not enhance the accessible density range, whereas a combination of gas puffing and pellet refuelling can lead to plasma densities far beyond the Greenwald limit. This is demonstrated in Fig. 9, where the temporal evolution of a pair of discharges is shown. During these discharges (#6522,#6523, I_P=1.0MA, B_t=2.5T, ∇B drift upwards,

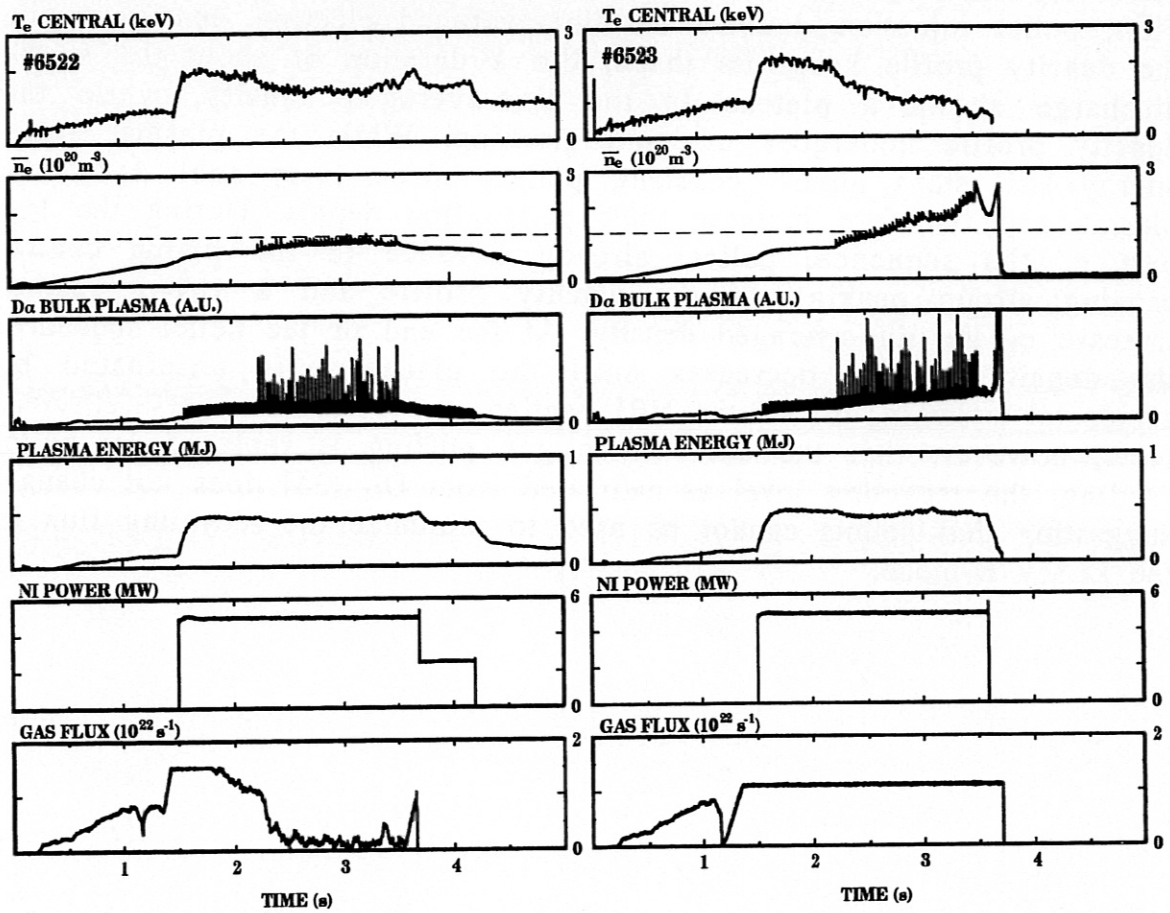

Fig. 9: Temporal evolution of a pair of type I ELMy H-mode discharges with either gas puff or pellet refuelling (#6522) or combined refuelling (#6523). Enhancement of the line-averaged density beyond the empirical Greenwald limit (indicated by broken line) was only achieved for the case of combined refuelling by gas puff and pellet injection.

q_{95}=3.9, P_{NI}=5MW) a pellet sequence was injected at a repetition rate of 30 Hz for a duration of 1.3 s. While pellet injection completely replaces gas puffing into the plasma for the one discharge (#6522), gas puffing was maintained during the pellet sequence for the other one (#6523). For the case where pellets replace the gas puff at t = 2.25 s, only a slight increase in density takes place during the pellet sequence although the particle flux delivered by the pellets is more than three times that of the previous gas puff. In this discharge, $\overline{n_e}$ only approaches the empirical Greenwald limit ($\overline{n}_{e,Gw} = \frac{I_p}{a^2 \pi}$, 1.28 x 10^{20} m^{-3} for this discharge, dashed line in Fig. 9). With the combination of gas puff and

pellet injection, the influence on the discharge can be much stronger. First, pellet injection doubles the line-averaged electron density, while the density profile keeps its shape. For a duration of about 0.3 s, the discharge shows a plateau in the line-averaged density, while the density profile undergoes moderate peaking. While the plasma stored energy still stays almost constant, pellets successively cool down the plasma and therefore increase their penetration depths. During the last part of the sequence, pellets already advance to the plama centre, causing strong peaking of the density profile and a strong further increase of the line-averaged density. At the end of the pellet sequence, the density rapidly decreases until the discharge is terminated by accidental switching-off of the NBI heating.
Note, however, that the case where gas puffing is replaced by pellet fuelling, the recycling level as estimated from D_α [34] does not change, suggesting that pellets cannot be used to minimize the recycling flux in the ELMy H-mode.

4. DISCUSSION AND MODELLING

4.1 Prompt particle loss in hot plasmas

The increasing shift of the effective ablation profile to the plasma edge (compared with the dynamic ablation profile) and the decreasing fuelling efficiency for growing heating power might be caused by fast radial transport. The shift of ablated pellet material is already finished about 1ms after injection, and so this fast radial transport must take place on a time scale much faster than the diffusive time scale τ_{diff} for density. The particle diffusivity in the plasma, also monitored by the density decay of pellet-fuelled plasmas, is of the order of $1 m^2/s$ or less [19], while ordinary diffusivity suggests only a modest diffusion of the density in the time between injection and the post-pellet density profile measurement. It is possible, though, that the local perturbation of the pellet may cause additional transport on a timescale much shorter than τ_{diff}.

The appearance of such rapid radial transport has already been predicted by a study on the neutral gas plasma shielding of ablating pellets passing through a hot plasma [35]. It is shown that the plasma pressure within the ablation cloud can rise to relatively high values within a few μs since the heat flux carried mainly by the hot electrons into the cloud causes a much more rapid temperature increase there than is compensated by expansion of ablated particles along the field lines. Whereas the classical local thermal flux q [36] (taking into account non-local effects does not substantially alter the behaviour [35])

$$q = - \chi_e \frac{\partial T_e}{\partial x} \approx T_e^{5/2} \frac{\partial T_e}{\partial x}$$

into the ablation cloud strongly rises ($\approx T_e^{7/2}$) with increasing plasma temperature, thermal expansion of ablated particles is only very modestly enhanced ($v_e \approx T_e^{1/2}$). Consequently, the toroidal ß increase within the ablation cloud takes place within a much shorter time for high ambient plasma temperatures - and therefore higher P_{NI} - than for colder ones. We estimate - by assuming dimensions of the ablation clouds as typically observed by high-speed photographic techniques [18,37] and adopting our measured ablation rates - the evolution of a ß value of the order of unity to be possible within a few μs for typical ambient plasma conditions at a high applied neutral injection power. For such a rapid change in the local ß, however, a massive local perturbation of the magnetic field and a substantial change of the confinement properties of the background plasma may occur [38]. Analyzing the

expansion and movement of a high-ß "plasmoid" in a magnetically confined plasma showed that the rediffusion of the magnetic field into the plasmoid can last for several tens of μs and hence the plasmoid is subject to polarization-induced drift forces [39]. An estimation of the diamagnetic drift force for the conditions considered here yielded an acceleration of the order of 10^{10}m/s^2. This is capable of shifting the plasmoid over a few cm within a few μs into the drift direction towards the low-field side of the torus. These conclusions and estimations are supported by the observations of a prompt particle flux from the plasma following pellet injection, the video observations indicating the expelled material to be still confined within a flux tube (see Fig. 4), and finally also by high-speed framing camera observations of the pellet ablation dynamics performed at TEXT [37]. There, the expelling of the cigar-shaped ablation region at a velocity of about 4 x 10^3m/s is reported in a direction anti-parallel (to the low-field side of TEXT) to the pellet motion, shifting the plasmoid about 2cm within 3μs.
Thus, we speculate that the occurrence of a high-ß plasmoid causing a fast radial particle drift, strongly increasing with rising plasma temperature, results in a strong degradation of the fuelling efficiency with increasing heating power. However, further experimental investigations are needed for conclusive confirmation of this view.

4.2. Pellet induced ELMs and ELM induced particle loss

The modelling presented in this section was done to achieve a qualitative explanation of the ε_f H-mode degradation by means of a simple physical picture. Basic aim of the modelling was to reproduce the two main experimental features, i.e. first, the release of an ELM by each pellet and, second, the increase in ε_f with growing pellet penetration depth. The model used for this purpose is basically identical with the model used for modelling the dynamic behaviour of the L-H transition [40]. The code simultaneously solves the radial 1D diffusion equations for both the energy

$$\frac{\partial T}{\partial t} = \frac{2}{3}\frac{\partial}{\partial r}\left(\chi \frac{\partial T}{\partial r}\right) + \frac{1}{n}\left(\frac{2}{3}\chi + D\right) \frac{\partial T}{\partial r}\frac{\partial n}{\partial r}$$

and one species of particles

$$\frac{\partial n}{\partial t} = \frac{\partial D}{\partial r}\frac{\partial n}{\partial r} + D\frac{\partial^2 n}{\partial r^2}$$

in cylindrical geometry. Boundary conditions were chosen via the derivatives $\frac{1}{\lambda_n} = \frac{\partial n(r)/\partial r}{n(r)} = \text{const}$ and $\frac{1}{\lambda_T} = \frac{\partial T(r)/\partial r}{T(r)} = \text{const}$ at the outer edge of the modelled region, with values from appropriate experimental profiles being adopted. The same was done for choosing the starting conditions. Non-pellet particle refuelling is introduced as ionization of a permanent influx of neutrals from the outer edge, energy deposition as heat flux from the inner edge of the modelled area. Pellet particle deposition is introduced into the code as an adiabatic instantaneous event. Taking into account earlier experimental findings [41], transport properties of the H-mode are modelled by a transport barrier zone of radial extent δ in which the transport is reduced. For simplicity, diffusion coefficients were assumed to show no variation with t or r besides the increased transport in the barrier zone during the ELM phase. Within the transport barrier zone, D_{min} and χ_{min} were assumed during the H-mode, and D_{max} and χ_{max} while an ELM is present. For the region inside the barrier, D_{max} and χ_{max} are valid for all the time. A typical set used was $D_{max}=1\,m^2/s$, $D_{min}=0.1\,m^2/s$, $\chi_{max}=3\,m^2/s$, and $\chi_{min}=1\,m^2/s$; values are chosen according to different transport analyses performed for ASDEX Upgrade [42]. The release of an ELM event is triggered in the model when the maximum plasma pressure gradient within the boundary layer exceeds a critical value. This model assumption may be related to the experimental observation that type I ELMs always seem to appear at the ideal ballooning limit [43]. A return to H-mode transport conditions happens when the plasma pressure gradient has fallen everywhere in the boundary layer below a value of a fraction of the critical ELM trigger value or, alternatively, when a certain time period has elapsed. The results shown here are obtained by means of the first option, but applying fixed ELM periods does not significantly change the results. The model was adjusted to the experiment by means of several parameters. Besides the appropriate choices of the transport coefficient, λ_n and λ_T at the outer edge and the density and temperature derivatives at the inner edge of the spatial domain of the code, the particle and heat influxes were chosen to reproduce experimental values measured for particle and energy losses resulting from an ordinary ELM. For the width of the transport barriers, δ, a value of 5cm was chosen because the modulation depths in the temperature profiles, as measured by the ECE [44] at high temporal resolution (up to 16μs), were thus fitted very well in the model.

Results of code runs without (upper) and with pellet "injection" (lower) are shown in Fig. 10. The left parts of the figure show the particle content in the model domain, the right parts the particle flux leaving the

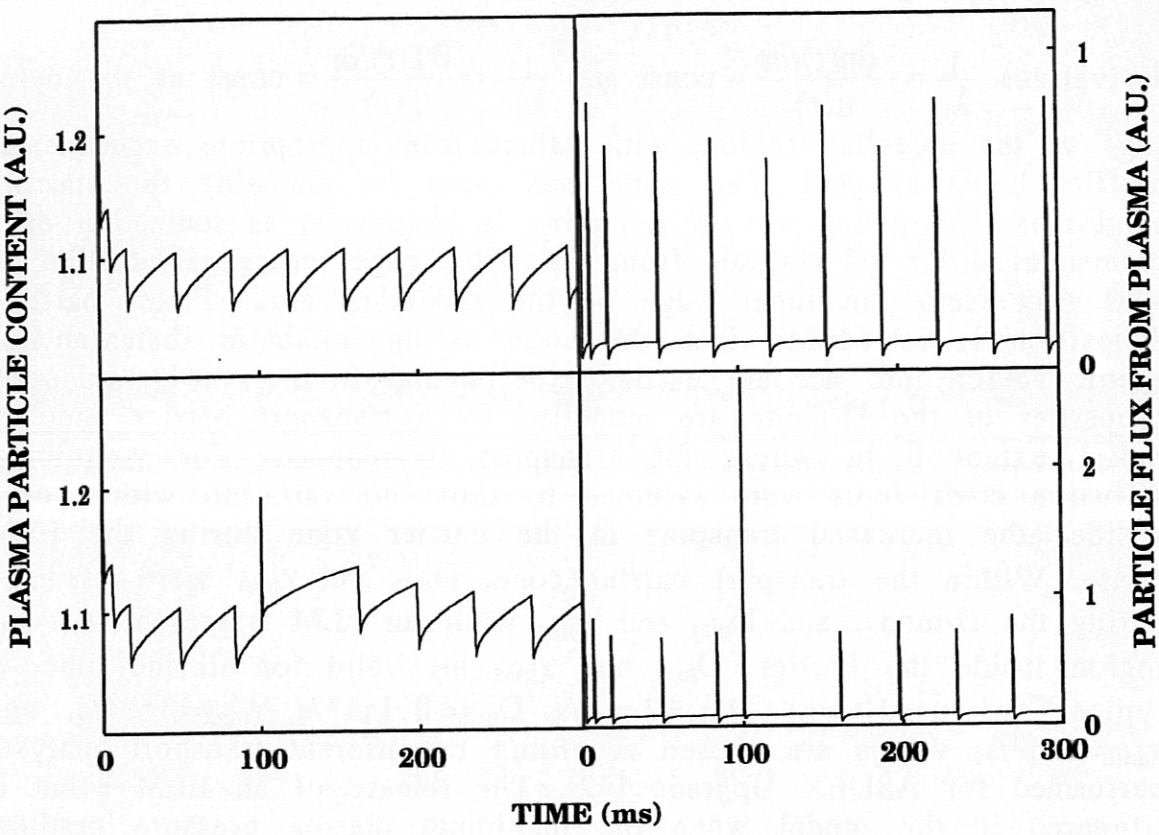

Fig. 10: Temporal evolution of particle inventory (left) and outflux (right) calculated by the transport code. Unperturbed evolution (upper) ending up in a stable periodic situation; additional particle deposition by a pellet at the time indicated causes an almost immediate release of an ELM by the pellet. For the adopted deposition profile (5cm penetration depths) the strong reduction of the pellet fuelling efficiency by the pellet-induced ELM is obvious.

plasma via the outer boundary. For the unperturbed simulation, a stable repetition period is established after some time. During a period - its duration being mainly determined by the heat and particle influxes applied in the simulation - the particle inventory continuously increases, while the flux from the plasma is rather weak and the profiles steepen in the transport barrier zone. Finally, the pressure gradient there exceeds its critical value and an ELM is released. During the ELM event, a strong loss of particles occurs, reducing the particle inventory and causing strong particle and heat fluxes from the plasma. The ELM smoothens the profiles in the edge region and a substantial decrease in n(r) and T(r) profiles takes place within a region about 15cm wide at the

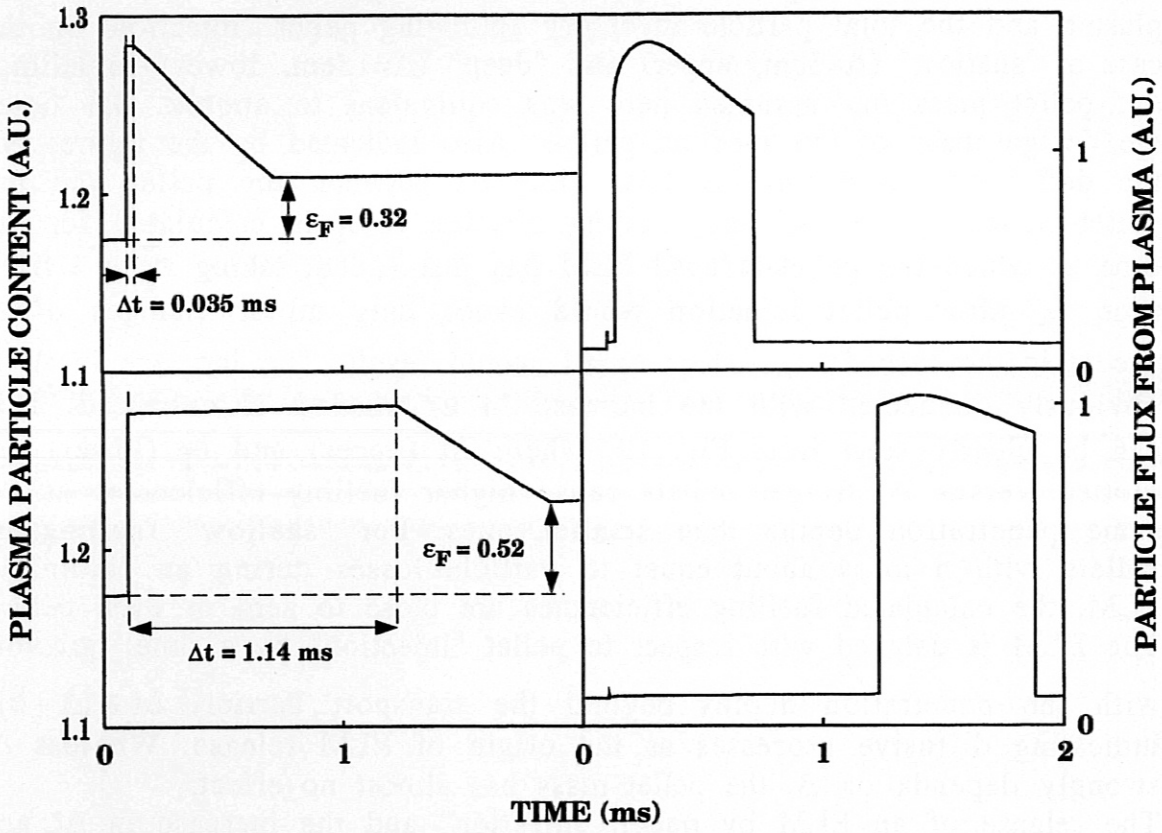

Fig. 11: Temporal evolution of particle inventory (left) and outflux (right) calculated by the transport code for "shallow" (Δ=5cm, upper) and "deep" (Δ=15cm, lower) penetration; also indicated is how the values for the delay time Δt between pellet and pellet-induced ELM and the fuelling efficiency are taken. The pellet mass m_p adopted here was approximately equivalent to the particle inventory enhancement introduced by a medium pellet in strongly heated ($P_{NI} > 5\,MW$) discharges.

outer edge of the model domain. An identical run performed with the additional deposition of a single pellet (Δ=5cm) at the time indicated showed an almost immediate release of a very strong particle outflux removing most of the particles just delivered by the pellet. Due to the altered pressure profile - the pellet induced a cooling wave travelling faster into the plasma than the density blob - the next ELM is somewhat delayed. Relaxation to the pre-pellet situation is re-established after a few "regular" ELM periods.

To explore the dependence of the fuelling efficiency on penetration depth and pellet mass, a series of code runs was performed with varying pellet deposition profiles at a fixed time in a specific scenario.

Figure 11 shows temporal evolutions of the particle fluxes from the plasma and the total particle inventory following pellet "injection" in the case of "shallow" (Δ=5cm, upper) and "deep" (Δ=15cm, lower) refuelling; the pellet mass m_P assumed here was equivalent to approx. 0.3 times the design mass of our medium pellets. Also indicated by the figures are the definitions used for the delay time Δt between the pellet and the pellet-induced ELM and the fuelling efficiency. ε_f is calculated for the time at which the pellet-induced ELM has just ended; taking ε_f at a fixed time t_A after pellet injection would cause only minor changes of ε_f except in the case $\Delta t > t_A$, where $\varepsilon_f \approx 1$ would result. The increase in Δt is obviously connected with the increase in ε_f when Δ is enhanced. This can be clearly seen from Fig. 12, where Δt (upper) and ε_f (lower) are plotted versus Δ. Bigger pellets cause higher fuelling efficiencies at the same penetration depths than smaller ones. For "shallow" fuelling by pellets with a mass about equal to particle losses during an "ordinary" ELM, the calculated fuelling efficiencies are close to zero or even below. The ELM is delayed with respect to pellet "injection" by a time growing with the penetration depths beyond the transport barrier, $\Delta t \cong (\Delta - \delta)^2$, indicating diffusive processes as the origin of ELM release. Whereas Δt strongly depends on Δ, the pellet mass has almost no effect.
The release of an ELM by pellet "injection" and the increase in Δt and fuelling efficiency with growing pellet penetration depth can be understood by analyzing the temporal evolution of the pressure profile, following the pellet particle deposition. An instructive example is shown in Fig. 13, where the result from a code run performed for pellet mass m_P and Δ=16cm ("deep" penetration case shown in lower part of Fig. 11) is presented. In order to visualize the ongoing evolution with better transparency, the deviation of the local pressure $p(r,t)$ with respect to its pre-pellet value $p(r,t_0)$ is plotted in its temporal behaviour across the plasma radius. When the pellet is "injected", it cools down the plasma and increases the density within the deposition area. As this process is assumed to be adiabatic, the pressure profile is not altered instantaneously. However, strong changes of both the n(r) and T(r) profiles take place. Due to

$$\frac{\partial p(r)}{\partial t} = \frac{3}{2}\left[D'n'T + Dn''T + \frac{D}{r}n' + \left(\frac{2}{3}\chi + D\right)n'T'\right] + \frac{n}{r}\frac{\partial}{\partial r}\left(r\chi T'\right)$$

(primes denoting $\frac{\partial}{\partial r}$), the strong temperature and density gradients generated by pellet injection lead to a nonadiabatic evolution of the pressure profile driven by energy and particle diffusion. Although no

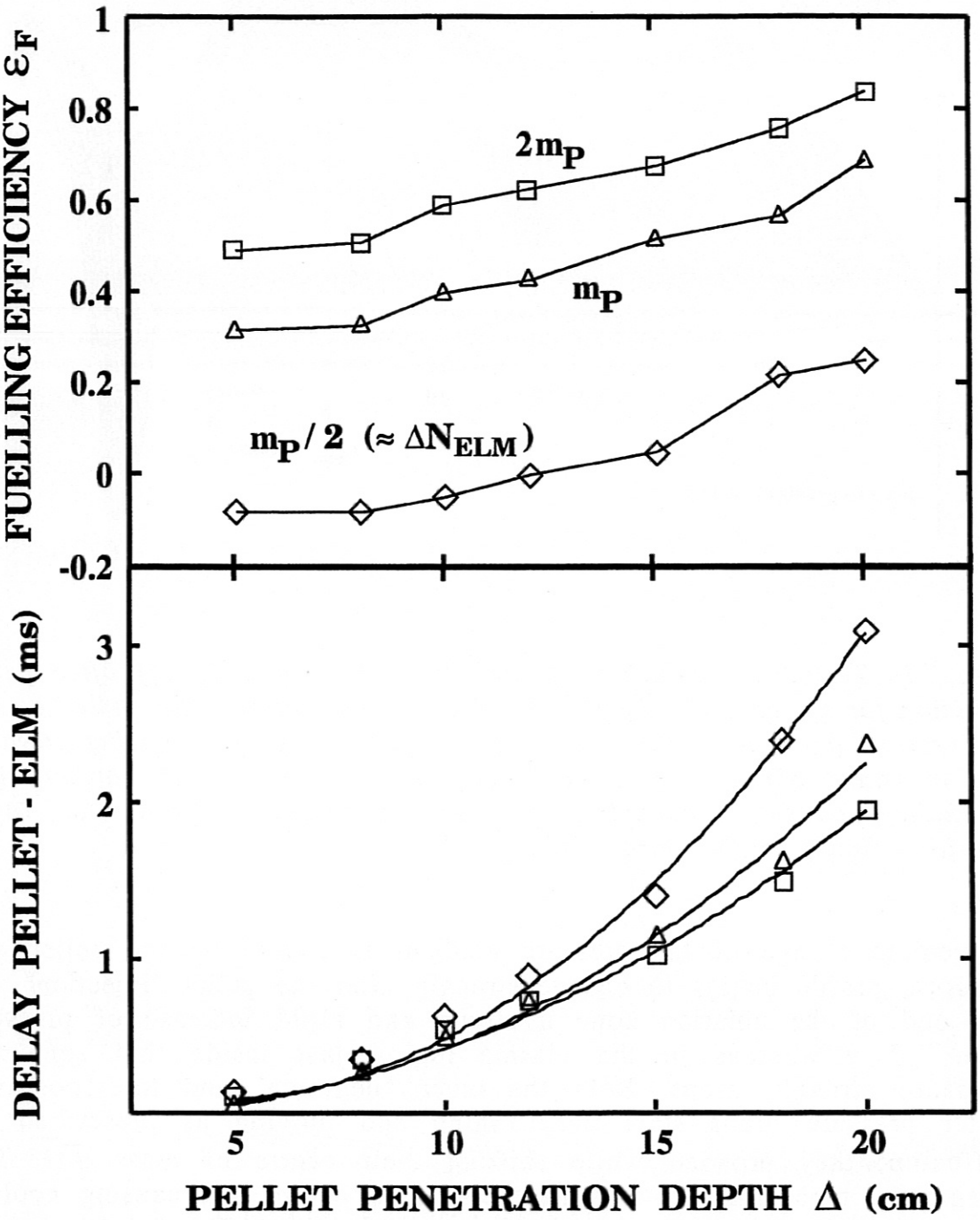

Fig. 12: ε_f (upper) and Δt (lower) versus Δ as calculated for different pellet masses.

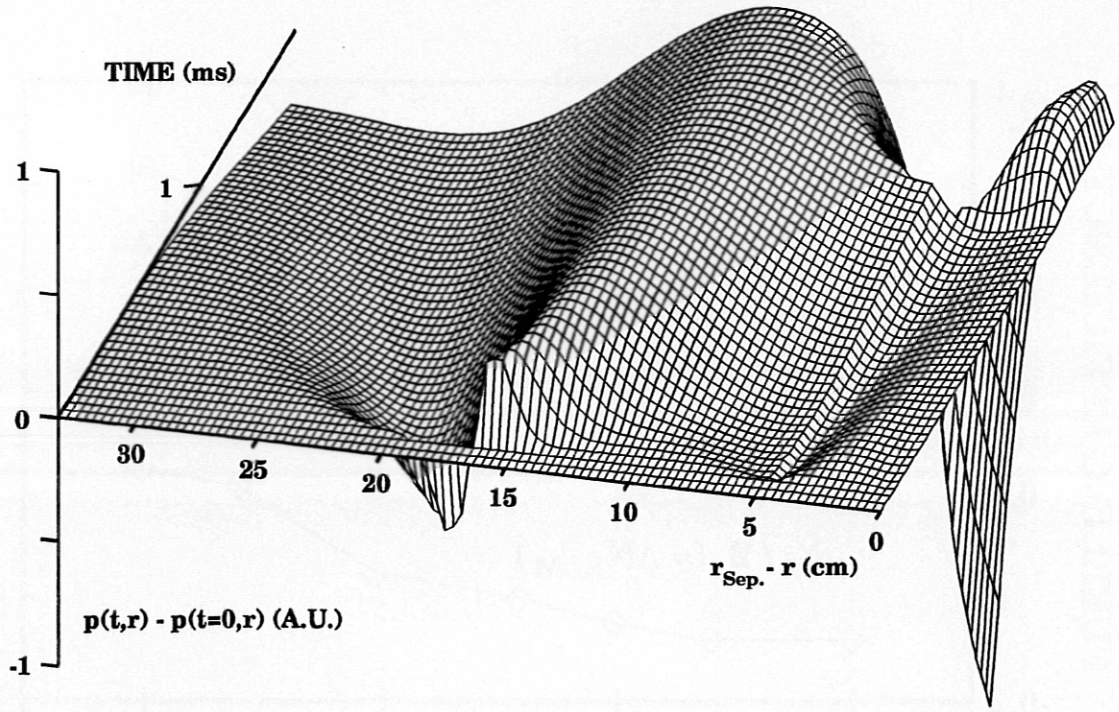

Fig. 13: Temporal evolution of the pressure profile ($p-p_0$) after pellet injection for the case of "deep" (Δ=16cm) penetration. The pellet causes a pressure pulse near the end of the deposition profile moving towards the transport barrier layer. Bottlenecking at the transport barriers inner boundary causes increasing pressure gradients within the layer, resulting finally in the release of an ELM.

immediate change of the pressure gradient is caused by the pellet, the pressure profile begins to change strongly after the pellet "injection". At the end of the ablation zone a strong and rapid increase of pressure takes place whereas in the plasma region just inside that zone the pressure strongly drops. Both the inner "negative" and the "positive" outer pressure blobs start transforming and moving as prescribed by diffusion: they broaden while shifting their centre of mass $\cong \sqrt{t}$. The "negative" blob, moving towards the plasma centre and causing cooling there, is of no further interest for our considerations. The "positive" blob moving to the plasma edge governs the further behaviour. When the pressure blob reaches the transport barrier, this bottleneck for the outward flux results in a pressure increase at the inner edge of the barrier and therefore also in a strong increase of the pressure gradient inside the barrier zone. According to our model, an ELM is thus finally

triggered. During the ELM event, when the transport barrier vanishes, strong gradients in the plasma edge region cause a strong outflux of particles and hence reduction of the particle inventory.
Due to the diffusive behaviour of the pressure blob generated near the end of the pellet particle deposition profile, the arrival of the pressure pulse in the edge transport barrier zone and hence the release of the ELM is delayed by a time Δt growing approximately proportionally to the square of the penetration depth. With growing Δ the increasing delay between particle deposition and the resulting breakdown of the transport barrier also allows longer-lasting diffusion of deposited particles towards the plasma centre. As both the experiment and simulation show the density and temperature not to be significantly affected by an ELM for locations more than about 15cm inside the separatrix, particles having reached this region are no longer endangered by the pellet-induced ELM. As a consequence, "deep" penetration both causes particle deposition mainly in a favourable region outside the ELM-affected region and allows particle diffusion into the unaffected region for a longer period. Contrary to this behaviour, "shallow" penetration causes particle deposition inside and just beyond the transport barrier layer, resulting in the release of an ELM before significant particle diffusion into the plasma can take place. With the breakdown of the transport barrier, the initial H-mode temperature and density profiles with steep gradients at the edge are subject to strong particle and energy losses from the edge region during an ELM event, because the H-mode profiles are not consistent with the edge transport coefficients during the ELM phase and transformation into smoothened profiles takes place. For the "shallow" fuelling case, most of the particles just deposited are thus quickly removed again and the fuelling efficiency is worse.
As the fast losses of the pellet-deposited particles takes place before radial diffusion causes the release of an ELM, their effect on the dynamic ablation profile must be taken into account when analyzing the modelling results in relation to the experiment. These processes, obviously taking place on a much shorter time scale than radial diffusion, were assumed not to affect the plasma properties for modelling on a time scale adequate for diffusive radial transport processes. Hence, fast radial transport processes were only taken into account for this modelling by using effective particle deposition profiles containing fewer particles than the initial pellet. The fuelling efficiencies calculated thus refer to the amount of particles deposited within the plasma after the fast loss process has ended, e.g. code runs were performed using an equivalent of 0.3 times the design masses of the pellets. Therefore, the fuelling efficiencies approaching unity that were achieved for "deep" pellet penetration in the modelling are equivalent to

the experimentally observed recovery of ε_f values in the H-mode to values obtained for L-mode conditions. Thus, the model is able to explain qualitatively the degradation of ε_f in the H-mode with decreasing penetration depths because it reproduces experimental observations of increasing fuelling efficiency with enhanced pellet penetration depth Δ. For a full quantitative analysis however, detailed knowledge of the fast radial transport processes and their influence on the ablation profile is required.

5. CONCLUSION

A wide variability of the deposition profile - achieved by variation of the pellet mass and velocity - in combination with pellet repetition rates variable up to 80Hz was found to yield optimum conditions for refuelling studies by pellet injection. The most favourable influence on both the particle and energy confinement is achieved by the pellets in the case of ohmic discharges (no additional heating power applied). Using pellets, the linear increase in τ_E with increasing $\overline{n_e}$ could be kept to about twice the value at which saturation occurred for gas puffing. Moreover, by causing peaked density profiles and as the density limit is governed by the edge density, pellet refuelling gives access to operational parameters not attainable by gas puffing.

Being almost unity in the ohmic case, fuelling efficiencies decrease with increasing heating power applied. This ε_f power deterioration is accompanied by loss of the favourable effect on confinement. For strongly heated plasmas (P_{NI}>5MW), no significant influence of pellet fuelling on τ_E is observed. The ε_f deterioration with power must be caused by a fast radial transport process occurring on a microsecond time scale, much faster than radial diffusion. We speculate that this fast radial drift results from the high plasma pressure occurring in the pellet ablation cloud, causing strong diamagnetic drift forces directed to the low-field side of the torus. This interpretation is supported by video observations showing that the particles lost from the pellet deposition profile are still confined within a hose expanding along the field lines and further by investigations of the ablation dynamics at high temporal resolution that show the release of an ablation cloud to the low-field side at a velocity in accordance with that estimated by the high-ß drift model.

Beyond the degradation of ε_f with increasing heating power, decreasing fuelling efficiencies were also found when the penetration depths were reduced. Whereas this effect only weakly occurs in the case of very shallow deposition in L-mode discharges, a strong effect was found during H-mode phases. For shallow fuelling of H-mode plasmas rather low or even zero fuelling efficiency was found; for increasing penetration depths an enhancement of ε_f takes place until almost the values obtained for the L-mode are re-established for "deep" fuelling. This behaviour is caused by the release of an ELM for each single pellet injected during an H-mode phase. A pressure pulse is formed near the end of the pellet deposition profile, diffusing towards the plasma edge. Bottlenecking of the pressure at the transport barrier during an H-mode phase causes strongly increasing pressure gradients inside the barrier and hence triggers an ELM event. For the case of "shallow" pellet particle

deposition, pellet-induced ELMs are triggered almost instantaneously after deposition and a high fraction of the particles located near the edge are again quickly removed during the breakdown period of the barrier layer. The advantage of "deep" penetration is a deposition profile containing most of the pellet particles within a region not affected by the ELM; morever, as the pellet-induced ELM is delayed with respect to the deposition, particles deposited near the edge can "escape" to the plasma interior from the regions affected.
With sufficient deep deposition, acceptable fuelling efficiencies can be obtained even for strongly heated H-mode plasmas. By applying adequate repetition rates significant density ramp-up was thus achieved when injecting pellet sequences. The obviously favourable refuelling scenario for such discharges is to use pellet injection combined with additional gas puffing. Thus, maximum values of $\overline{n_e} \approx 2.6 * 10^{20}$ were reached transiently, exceeding the Greenwald limit by a factor of two. However, in this case, a strong recycling flux occurs, making the idea of isotopic tailoring at least questionable in the ELMy H-mode at high density.
For further improving the refuelling scenario in order to achieve stable operation conditions, too strong cooling of the plasma by the pellets must be avoided. Therefore, it is necessary to adjust the heating power and/or the pellet injection rate to the actual plasma conditions. The new ASDEX Upgrade control system, already taken successfully into operation, will allow for this purpose in our next experimental campaign.

REFERENCES

[1] H. Nakamura, J. Dietz, and P. Ladd, Fusion Technology 28 (1995) 705.
[2] M. Gouge et al., Fusion Tech. 28 (1995) 1644.
[3] N. Greenwald et al., Nucl. Fusion 28 (1988) 2199.
[4] P.T. Lang et al., in Controlled Fusion and Plasma Physics (Proc. 22nd Eur. Conf. Bournemouth, 1995), Vol. 19C, Part II, European Physical Society, Geneva (1995) , 449.
[5] S.L. Milora et al., Nucl. Fusion 22 (1982) 1263.
[6] D.P. Schiessel et al., Nucl. Fusion 27 (1987) 1063.
[7] M. Kaufmann et al., Nucl. Fusion 28 (1988) 827.
[8] M.G. Bell et al., Nucl. Fusion 32 (1992) 1585.
[9] G.L. Schmidt et al., in Plasma Physics and Controlled Nuclear Fusion Research 1986 (Proc. 11th Int. Conf. Kyoto, 1986), Vol. 1, IAEA, Vienna (1987) 171.
[10] B.J.D Tubbing et al., Nucl. Fusion 31 (1991) 839.
[11] H. Zohm, Plasma Phys. Control. Fusion 38 (1996) 105.
[12] C. Andelfinger et al., Rev. Sci. Instrum. 64 (1993) 983.
[13] G. Neu et al., Fusion Technology (Proc. 18th Symp. Karlsruhe, 1994), Vol. 1, Elsevier Science, Amsterdam (1995) 675.
[14] K. Büchl, G.C. Vlases, W. Sandmann, and R.S. Lang, Nucl. Fusion 27 (1987) 1939.
[15] P.T. Lang et al., in Controlled Fusion and Plasma Physics (Proc. 21th Eur. Conf. Montpellier, 1994), Vol. 18B, Part I, European Physical Society, Geneva (1994) 306.
[16] F. Ryter et al., in Controlled Fusion and Plasma Physics (Proc. 21th Eur. Conf. Montpellier, 1994), Vol. 18B, Part I, European Physical Society, Geneva (1994) 330.
[17] M. Kaufmann et al., Plasma Phys. Control. Fusion, Vol. 35 Suppl. (12)B, (1993) 205.
[18] L.R. Baylor et al., in Controlled Fusion and Plasma Physics (Proc. 22nd Eur. Conf. Bournemouth, 1995), Vol. 19C, Part I, European Physical Society, Geneva (1995) , 113.
[19] L.R. Baylor et al., Nucl. Fusion 32 (1992) 2177.
[20] S.L. Milora, J. Fusion Energy 1 (1981) 15.
[21] C.T. Chang and K. Thomsen, Nucl. Fusion 24 (1984) 697.
[22] V. Mertens et al., Plasma Phys. Contr. Fusion 36 (1994) 1307.
[23] G.V. Pereverzev, Rep. IPP 5/42, Max-Planck-Institut für Plasmaphysik, Garching (1991).
[24] K.W. Gentle et al., Particle Transport in ASDEX Upgrade, Rep. IPP 1/282, Max-Planck-Institut für Plasmaphysik, Garching (1994).
[25] K.W. Gentle, O. Gehre, amd K. Krieger, Nucl. Fusion 32 (1992) 217.
[26] A. Weller et al., Phys. Rev. Lett. 59 (1987) 2303.

[27] G.L. Schmidt et al., in Plasma Physics and Controlled Nuclear Fusion Research 1984 (Proc. 10th Int. Conf. London, 1984), Vol. 1, IAEA, Vienna (1985) 45.
[28] P.K. Mioduszewski et al., in Plasma Physics and Controlled Nuclear Fusion Research 1984 (Proc. 10th Int. Conf. London, 1984), Vol. 1, IAEA, Vienna (1985) 257.
[29] R.J. Fonck et al., J. Nucl. Mater. 128&129 (1984) 330.
[30] A. Carlson et al., in Controlled Fusion and Plasma Heating (Proc. 15th Eur. Conf. Dubrovnik, 1988), Vol. 12B, Part III, European Physical Society, Geneva (1988) 1069.
[31] D.K. Owens et al., in Controlled Fusion and Pellet Injection and Toroidal Confinement (Proc. Tech. Comm. Mtg., Gut Ising, 1988), IAEA-TECDOC-534, IAEA, Vienna (1989) 191.
[32] H.W. Drawin and A. Géraud, Nucl. Fusion 29 (1989) 1681.
[33] A. Kallenbach et al., Characteristics of radiative boundary discharges with different impurity injection conditions, Rep. IPP10/1, Max-Planck-Institut für Plasmaphysik, Garching (1996); submitted to Plasma Phys. Control. Fusion.
[34] G. Haas et al., in Controlled Fusion and Plasma Physics (Proc. 22nd Eur. Conf. Bournemouth, 1995), Vol. 19C, Part I, European Physical Society, Geneva (1995) , 321.
[35] M. Kaufmann, K. Lackner, L. Lengyel, and W. Schneider, Nucl. Fusion 26 (1986) 171.
[36] A. Temkin and J.C. Lamkin, Phys. Rev. 121 (1961) 788.
[37] R.D. Durst et al., Nucl. Fusion 30 (1990) 3.
[38] L.L. Lengyel, Phys. Fluids 31 (1988) 1577.
[39] L.L. Lengyel, Nucl. Fusion 4 (1977) 805.
[40] H. Zohm, Phys. Rev. Lett. 72 (1994) 222.
[41] The ASDEX Team, Nucl. Fusion 29 (1989) 1959.
[42] A. Kallenbach et al., Nucl. Fusion 35 (1995) 1231.
[43] P. Gohill et al., Phys. Rev. Lett. 61 (1988) 1603.
[44] H. Zohm et al., Plasma Phys. Control. Fusion 37 (1995) 437.